# SUPPLEMENTARY INFORMATION

# Origin of Non-Conservative Circular Dichroism in the CP29 Antenna Complex of Photosystem II

Dominik Lindorfer*, Frank Müh and Thomas Renger

Institute of Theoretical Physics, Department of Theoretical Biophysics, Johannes Kepler University Linz, Altenbergerstr. 69, 4040 Linz, Austria

E-mail: dominik.lindorfer@jku.at

## 1 Details of line-shape functions

The line-shape function in eq. 17 and 18 of the main text is given as

$$D_{M_d}(\omega) = \frac{1}{2\pi}\int_{-\infty}^{\infty} dt e^{i(\omega-\tilde{\omega}_{M_d0})t}\ e^{G_{M_d}(t)-G_{M_d}(0)}\ e^{-|t|/\tau_{M_d}} \tag{1}$$

Here, the transition frequency from the ground state to the $M$th exciton state in domain $d$ is denoted as $\tilde{\omega}_{M_d0}$, which is shifted due to exciton-vibrational coupling from the exciton transition frequency $\omega_{M_d0} = E_{M_d}/\hbar$ by

$$\tilde{\omega}_{M_d0} = \omega_{M_d0} - \gamma_{M_dM_d}\frac{E_\lambda}{\hbar} + \sum_{K_d,M_d}\gamma_{M_dK_d}\tilde{C}^{(Im)}(\omega_{M_dK_d}) \tag{2}$$

containing the reorganization energy $E_\lambda$ in eq. 8 of the main text and the half-sided Fourier transform of the correlation function of site energy fluctuations $\tilde{C}(\omega)$. The real and imaginary parts of the latter are given as

$$\tilde{C}^{(\mathrm{Re})}(\omega) = 2\pi\omega\{(1+n(\omega))J(\omega) + n(-\omega)J(-\omega)\} \tag{3}$$

and

$$\tilde{C}^{(\mathrm{Im})}(\bar{\omega}) = \frac{1}{\pi}\mathcal{P}\int_{-\infty}^{\infty} d\bar{\omega}\frac{\tilde{C}^{(Re)}(\bar{\omega})}{\bar{\omega}-\omega} \tag{4}$$

respectively, where $\mathcal{P}$ denotes the principal part of the integral. Please note that $\tilde{\omega}_{M_d0}$ in eq. 2 is the transition frequency of the isolated exciton domain $d$, since the diagonal elements of the perturbation operator $V_{Q_y,he}$ in eq. 2 of the main text are zero and hence there is no first-order contribution to the transition energies. Lifetime broadening due to exciton relaxation is described through the inverse dephasing time $\tau_{M_d}^{-1}$

$$\tau_{M_d}^{-1} = 2\sum_{K_d}\gamma_{M_dK_d}\tilde{C}^{(Re)}(\omega_{M_dK_d}) \tag{5}$$

and $\omega_{M_dK_d}$ is the transition frequency from exciton state $|M_d>$ to $|K_d>$ of domain $d$. The function $\gamma_{M_dK_d}$ is an electronic overlap factor between exciton states $|M_d^{(0)}>$ and $|K_d^{(0)}>$

$$\gamma_{M_dK_d} = \sum_{m_d} \left(c_{m_d}^{(M_d)}\right)^2 \left(c_{m_d}^{(K_d)}\right)^2 \tag{6}$$

The time-dependent function $G_{M_d}(t) = \gamma_{M_dM_d} G(t)$ in eq. 1 describes the excitation of the vibrational sidebands, where $G(t)$ is given as

$$G(t) = \int_0^\infty d\omega \{(1+n(\omega))J(\omega)e^{-i\omega t} + n(\omega)J(\omega)e^{i\omega t}\} \tag{7}$$

and contains the spectral density $J(\omega)$ and the Bose-Einstein distribution function $n(\omega)$

$$n(\omega) = \frac{1}{e^{\hbar\omega/k_BT} - 1} \tag{8}$$

that describes the mean number of excited vibrational quanta at temperature $T$. The shape of the spectral density has been estimated[1] from fluorescence line narrowing spectra of B777 complexes

$$J(\omega) = \frac{S_0}{s_1 + s_2} \sum_{i=1,2} \frac{s_i}{7!2\omega_i^4} \omega_i^3 e^{-(\omega/\omega_i)^{1/2}} \tag{9}$$

with $s_1 = 0.5$, $s_2 = 0.8$, $\hbar\omega_1 = 0.069$ meV and $\hbar\omega_2 = 0.24$ meV. The Huang-Rhys factor $S_0 = 0.5$ was obtained from the temperature-dependence of the absorption spectrum[2].

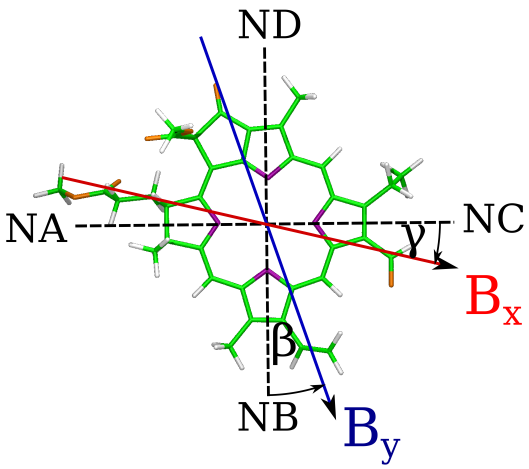


Figure S1: Illustration of the $N_B - N_D$ and $N_A - N_C$ axis of Chl. The transition dipole moments of $B_x$ and $B_y$ for extended dipole couplings are rotated by the angles $\beta$ and $\gamma$.

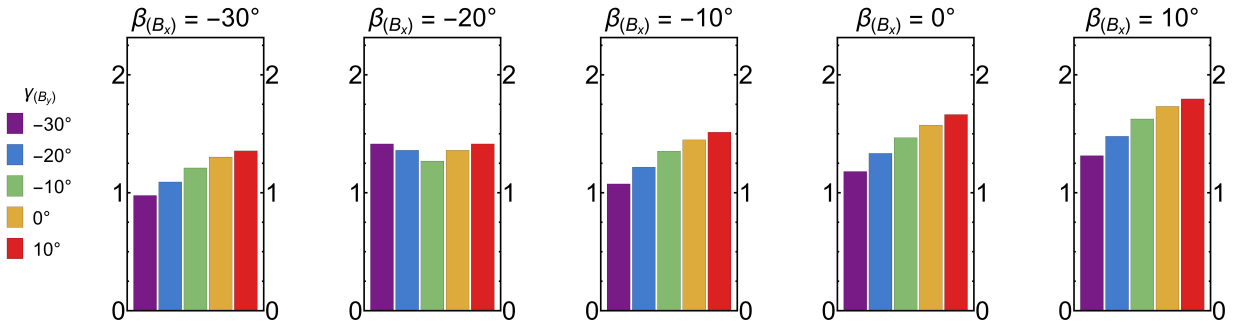


Figure S2: Comparison of the ratios $A_-/A_+$ of negative to positive area of the excitonic CD spectrum. Excitonic couplings are calculated using an extended dipole approximation for the $B_x$ and $B_y$ transitions which are rotated by the angles $\beta$ and $\gamma$ with respect to the $N_B - N_D$ and $N_A - N_C$ axes, respectively. All other transitions were described with atomic transition charges obtained from HF/CIS calculations.

Table S1: Transition dipole directions obtained with different QC methods. The angle $\beta$ for Chl *a* and Chl *b* is with respect to the $N_B - N_D$ axis as defined in Fig. S1. For carotenoids, the angle $\delta$ is given with respect to the direction of the polyene chain along the C7 − C27 axis. All angles given in degree.

| | Chl *a* | | | |
|---|---|---|---|---|
| | HF-CIS | CAM-B3LYP | B3LYP | BHHLYP |
| | $\beta$[°] | $\beta$[°] | $\beta$[°] | $\beta$[°] |
| $Q_y$ | 6.0 | 5.2 | 6.4 | 5.1 |
| $B_x$ | 77.5 | 88.7 | -8.8 | 88.8 |
| $B_y$ | -7.8 | 7.3 | 18.5 | 6.7 |
| $N_{x+xy}$ | 54.6 | 61.9 | 73.2 | 57.1 |
| | Chl *b* | | | |
| | HF-CIS | CAM-B3LYP | B3LYP | BHHLYP |
| | $\beta$[°] | $\beta$[°] | $\beta$[°] | $\beta$[°] |
| $Q_y$ | 14.1 | 10.2 | 9.1 | 9.1 |
| $B_x$ | 76.2 | 93.9 | 72.7 | 94.8 |
| $B_y$ | -11.9 | 24.4 | -29.7 | 26.8 |
| $N_{x+xy}$ | 46.4 | -69.0 | 79.1 | -63.1 |
| | Carotenoids | | | |
| | HF-CIS | CAM-B3LYP | B3LYP | BHHLYP |
| | $\delta$[°] | $\delta$[°] | $\delta$[°] | $\delta$[°] |
| Lut | 7.9 | 4.1 | 2.3 | 4.5 |
| Neo | 6.8 | 4.4 | 2.9 | 4.5 |
| Vio | 8.79 | 4.8 | 3.55 | 5.63 |

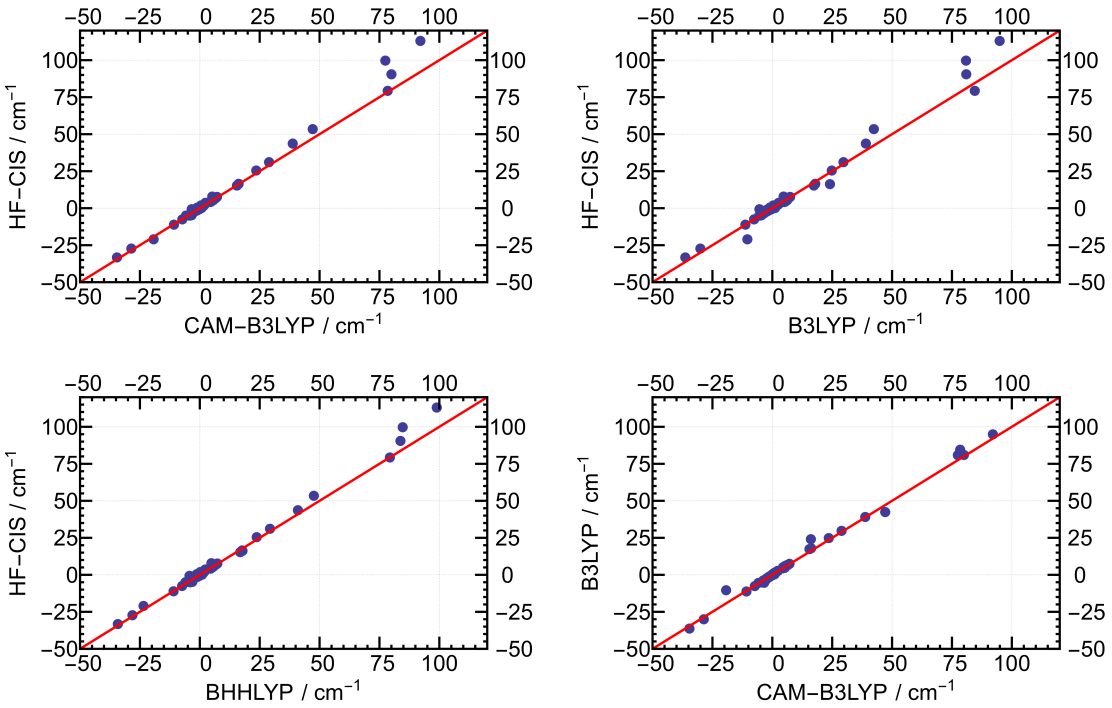


Figure S3: Comparison of Poisson-TrESP excitonic couplings of $Q_y$ transitions obtained from TD-DFT calculations using B3LYP, BHHLYP and the range separated CAM-B3LYP XC-functionals and the wavefunction based HF-CIS. The red lines represent perfect correlation.

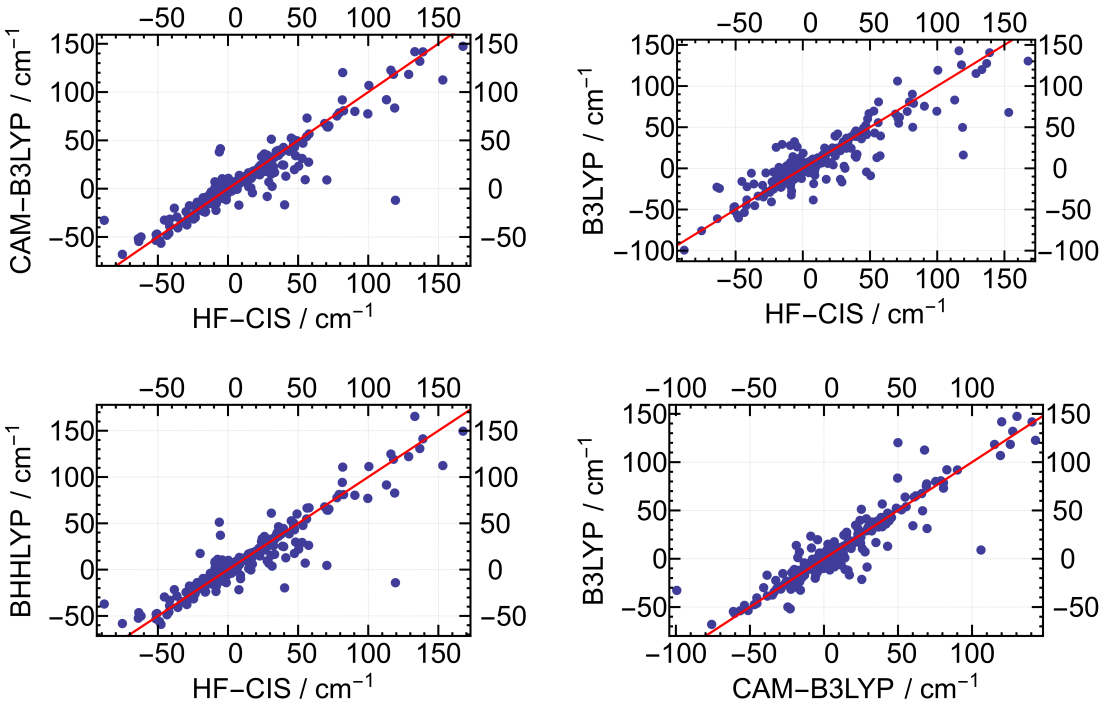


Figure S4: Comparison of Poisson-TrESP excitonic couplings between all pigments in CP29 obtained from TD-DFT calculations using B3LYP, BHHLYP as well as the range separated CAM-B3LYP XC-functionals with those obtained from the wavefunction based HF-CIS method. The red lines represent a perfect correlation.

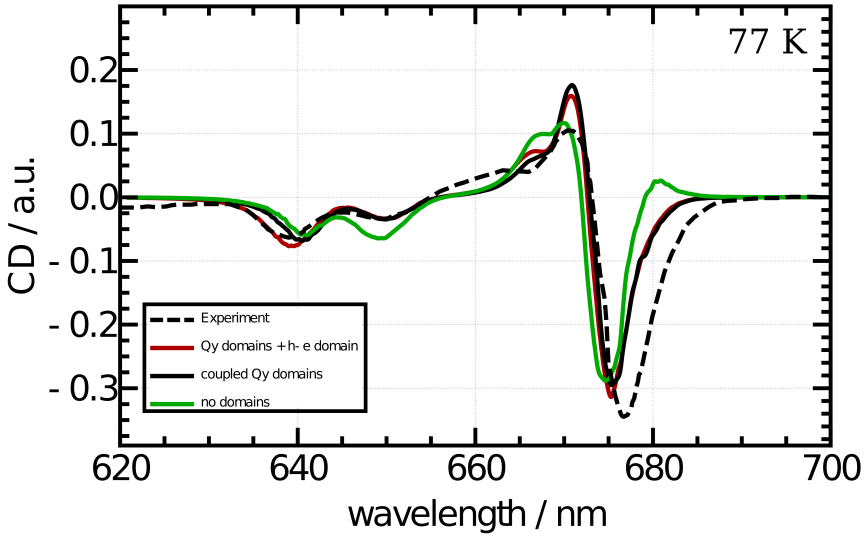


Figure S5: The red line shows the spectrum which is obtained by using domains for both $Q_y$ and high-energy transitions that are coupled in first order perturbation theory, as in Fig. 9 of the main text. The spectrum in black is obtained by diagonalizing an exciton Hamiltonian that contains the coupling between $Q_y$ domains and high-energy domains. The green line shows the spectrum that is obtained when no domains are introduced and thus one large exciton matrix is diagonalized. The dashed spectrum is the experiment[3] shown for comparison.

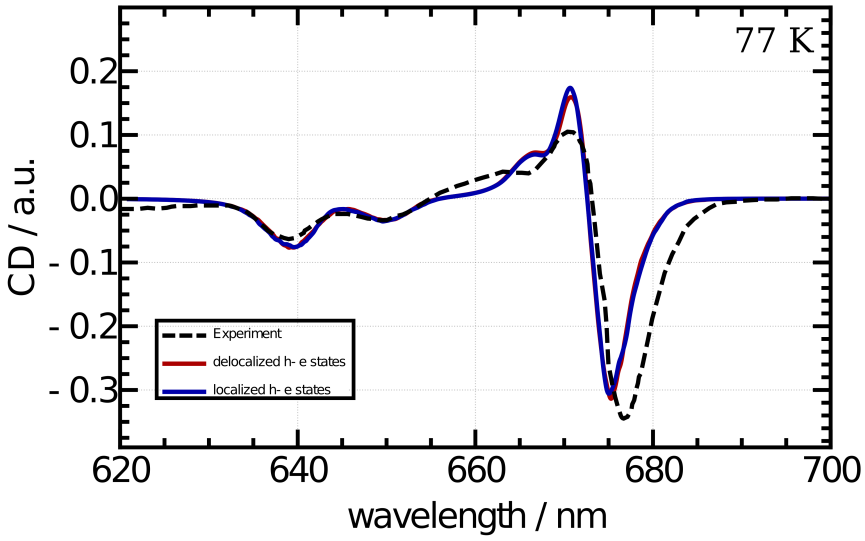


Figure S6: Comparison of spectra that are calculated by using domains for both $Q_y$ and high-energy transitions to the experiment[3]. The red line is obtained when allowing delocalization among high-energy transitions, as in Fig. 9 of the main text. The blue spectrum is obtained when all excitonic couplings between high-energy transitions are set to zero.

# References


[1] T. Renger and R. A. Marcus, *J. Chem. Phys.*, 2002, **116**, 9997–10019.

[2] F. Müh, D. Lindorfer, M. Schmidt am Busch and T. Renger, *Phys. Chem. Chem. Phys.*, 2014, **16**, 11848–11863.

[3] A. Pascal, C. Gradinaru, U. Wacker, E. Peterman, F. Calkoen, K.-D. Irrgang, P. Horton, G. Renger, R. van Grondelle, B. Robert and H. van Amerongen, *Eur. J. Biochem.*, 1999, **262**, 817–823.